

# Continuously-tunable slow and fast light using silicon microring add-drop filter with mutual mode coupling

Tao Wang<sup>1</sup>, Fangfei Liu<sup>1</sup>, Tong Ye<sup>1</sup>, Ziyang Zhang<sup>2</sup>, Jing Wang<sup>2</sup>, Yue Tian<sup>1</sup>, Min Qiu<sup>2</sup>, Yikai Su<sup>1</sup>

<sup>1</sup>State Key Lab of Advanced Optical Communication Systems and Networks, Department of Electronic Engineering, Shanghai Jiao Tong University, 800 Dongchuan Rd, Shanghai, 200240, China, yikaisu@sjtu.edu.cn

<sup>2</sup>Department of Microelectronics and Applied Physics, Royal Institute of Technology, Electrum 229, 16440, Kista, Sweden

**Abstract:** Continuously-tunable slow and fast light is experimentally demonstrated using silicon microring add-drop filter with mutual mode coupling. Pulse delay and advancement can be achieved by thermal tuning at the drop port of the resonator.

©2009 Optical Society of America

**OCIS codes:** (060.5530) Pulse propagation and temporal solitons; (130.0130) Integrated optics; (230.5750) resonators.

## 1. Introduction

To control the velocity of light has recently become an important topic. It offers the possibility of storing and buffering optical signals directly in the optical domain. Various tunable optical delay lines were studied, including stimulated Brillouin scattering (SBS) based fiber delay lines [1], photonic crystal structures [2], and silicon based nanowaveguides [3].

Silicon-on-insulator (SOI) platform has attractive advantages for all-optical devices due to its high refractive-index contrast between the silicon core and silica cladding, which allows strong optical confinement and enables ultra-compact photonic circuits. In particular, silicon microring-resonator based optical delay lines were proposed and large group delay was demonstrated [4]. However, continuously-tunable slow and fast light has not been realized in SOI device. In this paper, we experimentally demonstrate, for the first time to the best of our knowledge, continuously-tunable slow and fast light based on a silicon double-waveguide coupled microring resonator with mutual mode coupling.

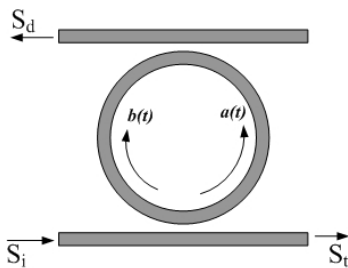


Fig.1: Schematic of microring coupled to double-waveguide. Wave  $S_i$  generates the counter-clockwise travelling mode  $a(t)$  in the ring. Clockwise travelling mode  $b(t)$  is generated by  $a(t)$  due to periodic roughness along the ring.

## 2. Theoretical analysis and simulations

The schematic of the double-waveguide microring is shown in Fig. 1. As discussed in Ref. [5], the incident wave  $S_i$  generates a counterclockwise traveling mode  $a(t)$ , which in turn induces a counter-propagation mode  $b(t)$  due to periodic structural roughness along the sidewall of the microring. Resonance splitting is caused by mutual coupling between these two traveling modes, which are related by the mutual coupling factor  $Q_u$ . To simplify the study of the double-waveguide coupled resonator, we assume that modes  $a$  and  $b$  have the same resonance frequency  $\omega_0$ , intrinsic quality factor  $Q_i$ ,

and coupling quality factors  $Q_e$  and  $Q_{e1}$  that correspond to the ring coupled to the lower and upper waveguides, respectively. The spectral response of the system is given by [5]:

$$T(\omega) = \frac{S_t}{S_i} = 1 - \frac{\omega_0}{2Q_e} \left[ \frac{1}{j(\omega - \omega_0 + \frac{\omega_0}{2Q_\mu}) + \frac{\omega_0}{2Q_i} + \frac{\omega_0}{2Q_e} + \frac{\omega_0}{2Q_{e1}}} + \frac{1}{j(\omega - \omega_0 - \frac{\omega_0}{2Q_\mu}) + \frac{\omega_0}{2Q_i} + \frac{\omega_0}{2Q_e} + \frac{\omega_0}{2Q_{e1}}} \right] \quad (1)$$

$$D(\omega) = \frac{S_d}{S_i} = \frac{\omega_0}{2} \sqrt{\frac{1}{Q_e Q_{e1}}} \left[ \frac{1}{j(\omega - \omega_0 + \frac{\omega_0}{2Q_\mu}) + \frac{\omega_0}{2Q_i} + \frac{\omega_0}{2Q_e} + \frac{\omega_0}{2Q_{e1}}} + \frac{1}{j(\omega - \omega_0 - \frac{\omega_0}{2Q_\mu}) + \frac{\omega_0}{2Q_i} + \frac{\omega_0}{2Q_e} + \frac{\omega_0}{2Q_{e1}}} \right] \quad (2)$$

It can be seen from Equation (1) and (2) that the traveling mode is split into two resonance frequencies, i.e.,  $\omega_0 - \omega_0/(2Q_\mu)$  and  $\omega_0 + \omega_0/(2Q_\mu)$ . According to Eq. (1), we plot the transmission spectra for three cases of  $Q_u = 2.7 \times 10^4$ ,  $Q_u = 1.9 \times 10^4$ , and  $Q_u = 1.4 \times 10^4$ , respectively, when  $Q_i = 2.6 \times 10^5$ ,  $Q_e = Q_{e1} = 6 \times 10^4$ , as shown in Fig. 2. It clearly illustrates that resonance splitting gradually enhances for both the through port and the drop port with the decreasing of  $Q_\mu$ . As discussed in [6], dispersion-induced group delay is defined as  $\tau_g = -d\Phi(\omega)/d\omega$ . Pulses will be delayed/advanced through this system if  $\tau_g$  has a positive/negative value, respectively. We plot the delay time as a

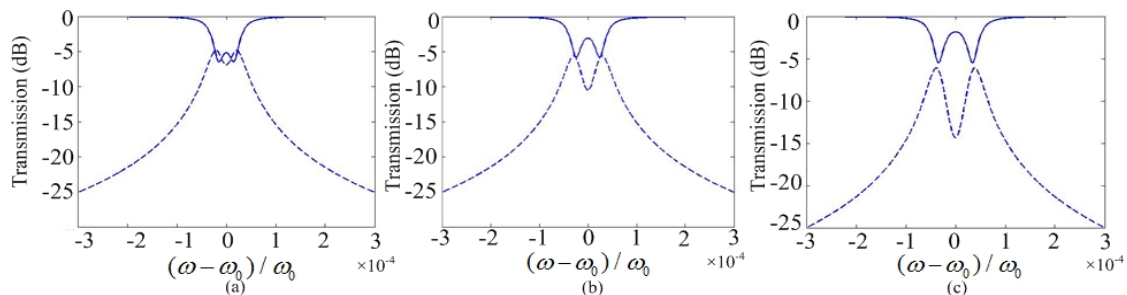


Fig.2: Simulated transmission spectra for through port (solid line) and drop port (dashed line), respectively. a)  $Q_\mu = 2.7 \times 10^4$ ; b)  $Q_\mu = 1.9 \times 10^4$ ; c)  $Q_\mu = 1.4 \times 10^4$ .

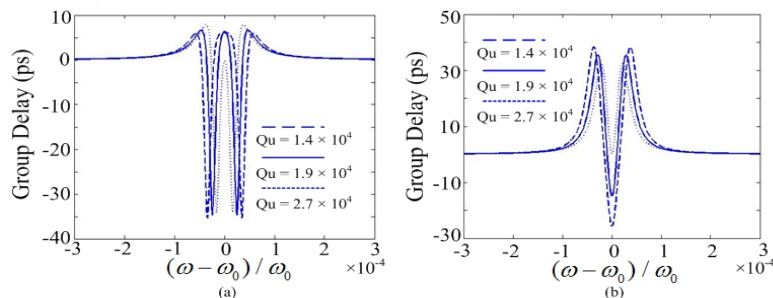


Fig.3: Simulations of group delays with respect to the normalized frequency detuning for the through port (a) and the drop port (b), respectively.

function of normalized frequency detuning, as shown in Fig. 3. For the through port, Fig. 3(a) shows that  $\tau_g$  becomes negative and its absolute value increases significantly with the normalized frequency approaching each split-resonance, which means that pulse advancement is achieved at split-resonances. The variation of group delay appears differently at the drop port, though, as shown in Fig. 3(b). Maximal pulse delay can be obtained at the two split resonances and is almost unaffected by the  $Q_\mu$  variation. However, as the frequency is detuned towards the middle of the two resonances,  $\tau_g$  reduces and changes to negative value. This implies that pulse propagation can be continuously tuned from delay to advancement. Moreover, the absolute value of  $\tau_g$  increases with the decreasing of  $Q_\mu$ . Therefore, the more significant the resonance splitting is, the more pulse advancement is achieved at the drop port of the resonator. Since the resonance splitting is determined by  $Q_\mu$ , i.e., the roughness along the sidewall of the microring, large pulse advancement can be realized by enhancing the sidewall roughness during fabrication procedure.

### 3. Experimental setup and results

Fig. 4(a) shows the scanning electron microscope (SEM) photographs of the resonator used in the experiment with a radius of  $20 \mu\text{m}$ . The ring/waveguide cross section is  $450 \times 250 \text{ nm}^2$  with an effective area of  $0.1 \mu\text{m}^2$  for the transverse-electric (TE) mode. The microring is side-coupled to the waveguides with an air gap of  $120 \text{ nm}$ . The transmission spectra of the resonator is measured around the resonance at  $1552.5 \text{ nm}$  and depicted in Fig. 4(b). We use return-to-zero (RZ) pulses as the probe signal in the experiment.

The experimental setup is depicted in Fig. 5. RZ pulses are generated by two cascaded Mach-Zehnder modulators (MZMs). The first MZM is driven by a 5-Gb/s pseudo-random bit sequence signal, and the second one is used as a

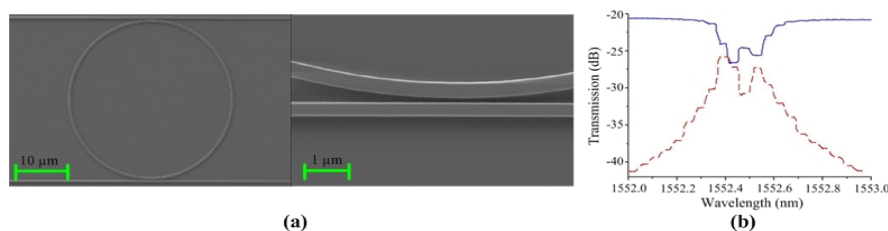


Fig.4: (a) The SEM photos of the silicon microring add-drop filter with a radius of  $20 \mu\text{m}$  and a zoom-in view of the coupling region. (b) Transmission spectra of the resonator around  $1552.5 \text{ nm}$ , which is measured at the through port (solid line) and the drop port (dashed line), respectively. (Resolution:  $0.01 \text{ nm}$ )

pulse carver driven by a sinusoidal signal with the same rate as the data. We tune the wavelength of CW light to measure the pulse delay and advancement. As shown in Fig. 6(a), points A, B, C, and D correspond to four different wavelengths around the split resonances. Firstly, we set the signal wavelength off resonance (point A) and take the corresponding pulse waveform (curve A) with an oscilloscope, shown in Fig. 6(b). When the wavelength is tuned to one of the split resonances (point B), the pulse is delayed by  $\sim 36$  ps (Fig. 6(b), curve B). When the signal wavelength sits between split resonances (point C), we observe that the pulse is advanced by  $\sim 12$  ps (Fig. 6(b), curve C). The advancement would increase if the mutual coupling between the counter-propagation modes is enhanced. Similarly, when the wavelength is tuned to another split resonance (point D), pulse delay is also obtained (Fig. 6(b), curve D). To demonstrate continuous tuning by thermal control, a control light is amplified by a high power erbium-doped fiber amplifier (EDFA) followed by an attenuator to adjust the power. Through a 3-dB coupler, it is fed to the resonator system together with the RZ signal pulses. Initially, the control power is attenuated to  $\sim 30$  dBm and the wavelength of probe signal sits in the middle of two split resonances. The corresponding pulse waveform (curve A) is shown in Fig. 6(c). When the control power increases to 8.4 dBm, the resonances are red-shifted due to the thermal effect [7]. The RZ signal then shifts towards the left split resonance, which causes a delay of  $\sim 25$  ps (Fig. 6(c), curve B). Pulse delay further increases (Fig. 6(c), curve C) when the control power goes up to 13.5 dBm, making the wavelength of the RZ signal closer to the left split resonance. Comparing with the reference pulse, one can observe that pulse propagation is continuously tuned from advancement ( $\sim 6$  ps) to delay ( $\sim 29$  ps). The tunable range would be extended if the control power further increases.

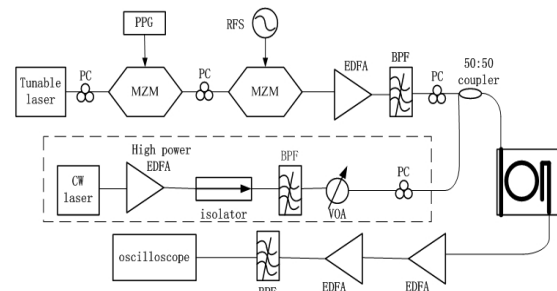


Fig. 5: Experimental setup for the optically tunable pulse delay and advancement using double-waveguide coupled resonator. CW: Continuous wave; PC: Polarization controller; PPG: Pulse pattern generator; RFS: Radio frequency synthesizer; EDFA: Erbium-doped fiber amplifier; BPF: Bandpass filter.

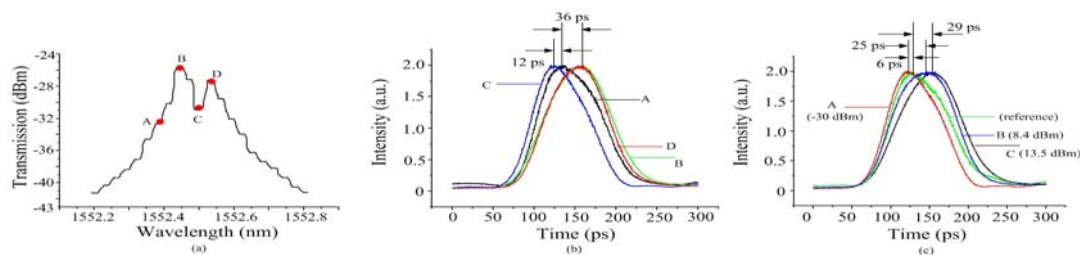


Fig. 6: (a) Measured transmission spectra of the drop port. Temporal waveforms of the RZ pulses with signal-wavelength detuning (b), and control-light thermal tuning (c), respectively.

#### 4. Conclusion

For the first time to the best of our knowledge, we experimentally demonstrate continuously-tunable slow and fast light in an SOI microring add-drop filter with mutual mode coupling. At the drop port of this system, pulse delay of  $\sim 29$  ps and advancement of  $\sim 6$  ps are obtained by thermal tuning the resonances.

**Acknowledgement:** This work was supported by the NSFC (60777040), Shanghai Rising Star Program Phase II (07QH14008), Swedish Foundation for Strategic Research (SSF) through the Future Research Leaders program, the SSF Strategic Research Center in Photonics, and the Swedish Research Council (VR).

#### References

- [1]. K.Y. Song, M.G. Herraes, and L. Thevenaz, "Long optically controlled delays in optical fibers," *Opt. Lett.*, 30, pp. 1782-1784(2005).
- [2]. Baba T, "Slow light in photonic crystals," *Nat. Photon.*, 2, pp. 465-473(2008).
- [3]. Y. Okawachi, M. Foster, J. E. Sharping, A. L. Gaeta, Q. Xu, M. Lipson, "All-optical slow-light on a photonic chip," *Opt. Express*, 14, pp. 2317 - 2322(2006).
- [4]. F. Xia, L. Sekaric, and Y. Vlasov, "Ultracompact optical buffers on a silicon chip," *Nat. Photon.*, 1, pp. 65-71(2007).
- [5]. Z. Zhang, M. Dainese, L. Wosinski, and M. Qiu, "Resonance-splitting and enhanced notch depth in SOI ring resonators with mutual mode coupling," *Opt. Express*, 16, pp. 4621-4630(2008).
- [6]. G. Lenz, B. J. Eggleton, C.K. Madsen, and R.E. Slusher, "Optical delay lines based on optical filters," *IEEE J. Quantum Electron.*, 37, pp. 525-532(2001).
- [7]. Q. Xu, and M. Lipson, "Carrier-induced optical bistability in silicon ring resonators," *Opt. Lett.*, 29, pp. 341-343(2006).